Robust Active Damping in *LCL*-filter based Medium-Voltage Parallel Grid-Inverters for Wind Turbines

Rafael Peña-Alzola, Javier Roldán-Pérez, *Member, IEEE,* Emilio Bueno, *Member, IEEE,* Francisco Huerta, *Member, IEEE,* David Campos-Gaona, *Member, IEEE,* Marco Liserre, *Fellow, IEEE,* Graeme Burt, *Member, IEEE*

Abstract—*LCL*-filter based grid-tie inverters require damping for current-loop stability. There are only software modifications in active damping, whereas resistors are added in passive damping. Although passive damping incurs in additional losses, it is widely used because of its simplicity. This article considers the active damping in medium-voltage parallel inverters for wind turbines. Due to cost reasons, only minimal software changes are allowed and no extra sensors can be used. The procedure must be robust against line-inductance variations in weak grids. Double-update mode is needed so the resonance frequency is under the Nyquist limit. The bandwidth reduction when using active damping is also required to be known beforehand. Moreover, the design procedure should be simple without requiring numerous trial-and-error iterations. In spite of the abundant literature, the options are limited under these circumstances. Filter-based solutions are appropriate and a new procedure for tuning the notch-filter is proposed. However, this procedure requires that the resistance of the inductors is known and a novel filter-based solution is proposed that uses lag-filters. The lag-filters displace the phase angle at the resonance frequency so that the Nyquist stability criterion is fulfilled. Simulations and experiments with a 100 kVA prototype validate the analysis.

Index Terms—*LCL*-filter, active damping, medium-voltage, voltage source converter, grid-tie inverter, line-inductance, notch-filter, lag-filter

I. INTRODUCTION

GRID-tie inverters require filters to limit the harmonic current injection to the grid. Compared to simple *L*-filters, *LCL*-filters result in lower overall inductance values. Passive damping uses resistors to achieve current-loop stability in the presence of the *LCL*-filter resonance, whereas active

R. Peña-Alzola was with the University of Alcalá, Spain and now he is with with the Rolls Royce UTC at the University of Strathclyde, Glasgow G1 1XQ, United Kingdom (e-mail: rafael.pena-alzola@strath.ac.uk).

J. Roldán-Pérez is with IMDEA Energy Institute, Parque Tecnolgico de Móstoles. 28935 Móstoles. Madrid, Spain. (e-mail: javier.roldan@imdea.org).

E. Bueno is with the Department of Electronics, University of Alcalá. Alcalá de Henares 28871 Madrid, Spain. (e-mail: emilio.bueno@uah.es).

F. Huerta was with the University of Alcalá, Spain and now he is with the Carlos III University of Madrid, 28911 Leganés, Spain (e-mail:fhuerta@ing.uc3m.es).

D. Campos-Gaona and G. Burt with the Department of Electronic and Electrical Engineering, University of Strathclyde. Glasgow G1 1XW United Kingdom (e-mail: davidcg@ieee.org;graeme.burt@strath.ac.uk).

M. Liserre is with the Institute for Power Electronics Electronics and Electrical Drives, Christian-Albrechts-University of Kiel, 24143 Kiel, Germany. E-mail: ml@tf.uni-kiel.de
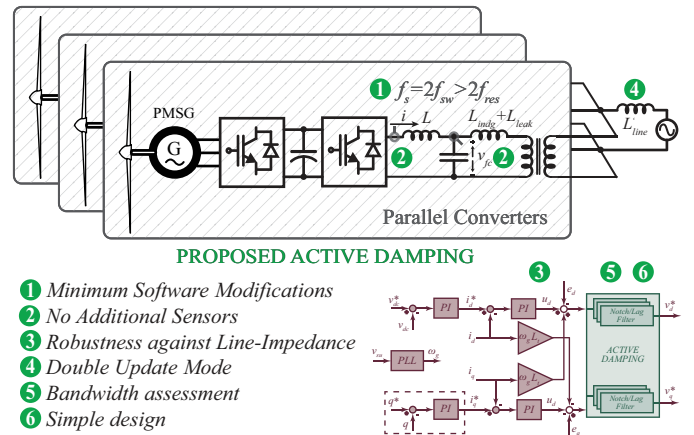

Fig. 1: Conceptual representation of the proposals.

damping requires only modifications in the control software. In spite of the additional losses, passive damping is widely used in the industry as it requires no change in the control software [1].

Much literature is devoted to the topic of active damping with many procedures cited. The method of the virtual resistor, originally proposed in [2], modifies the control algorithm to emulate the behavior of a damping resistor without physically adding it [3], [4]. This procedure requires additional sensors which depend on the position of the virtual resistor. The utilization of observers has been proposed in [5] to avoid using extra sensors at the expense of more controller complexity and computational load. Careful design of the digital controller must be exercised because of the computational and PWM delays. The analysis of the computational delay in the feedback loop of *LCL*-filter based inverters was analyzed in [6]–[8]. State-space control allows selecting the closed-loop poles in the proper locations [9]. However, it is difficult to pick up locations that result in acceptable phase and gain margins [10]. The use of an LQR regulator [11] may alleviate the latter issue by displacing the choice to the proper weighting coefficients. Moreover, multi-variable controllers require an elevated number of computations and they are difficult to re-tune for time-varying conditions [12]. In order to overcome the line-inductance variations that de-tune the active damping procedure, adaptive control techniques were

used in [13], [14]. Sliding mode control for *LCL*-filter based inverters is proposed in [15] and in [16], which includes a Kalman filter for magnitude estimation. In [17], it was shown that the feedback of the *LCL*-filter capacitor current to the voltage reference yields resonance damping. Another method for active damping consists in adding the capacitor voltage filtered by a lead-lag network [18], [19] or a high-pass filter [20] to the modulator voltage reference. Passing the reference voltage to the modulators through a notch-filter is a single loop strategy to achieve active damping [21]–[23]. The Posicast controller [24] is also an interesting technique using a single loop. The main disadvantage of these single loop strategies is that they are sensitive to changes in the resonance frequency due to line-impedance variations and may require parameter identification techniques [25] previous to being commissioned. Neural networks [26] and genetic algorithms [27] have also been applied for active damping.

The context of this article refers to *LCL*-filter based medium-voltage grid-tie parallel inverters for wind turbines. These power converters usually employ passive damping because of its simplicity. The requirements for the active damping procedure in this industrial application are the following:

1) *Minimum changes in the code* and *limited computation time*: to minimize the cost of software development and to avoid upgrading the DSP.
2) *No additional sensors* apart from the converter-side sensors for current-control and protection as they are relatively costly and can incur in re-engineering expenses.
3) *Robustness against line-impedance variations* as wind parks consists of parallel converters, and they are usually located in weak grids.
4) *Suitable for Double-update mode*, with the sampling frequency twice the switching frequency. This widely-used technique is used to increase the current-loop bandwidth and presents aliasing problems with certain active damping procedures. In the present case, double-update mode is mandatory to make the resonance frequency be under the Nyquist limit.
5) *Bandwidth assessment*, because of the limited switching frequency and so the limited bandwidth, one must know beforehand how much bandwidth will be sacrificed for using active damping.
6) *Simple design*, without requiring excessive trial-and-error iterations and simple to understand without requiring intensive training hours for the company engineers.

Procedures based on the state-space [9], [10], observers [5], LQR [11], [12] and Kalman filters [16] require matrix operations and cannot meet the requirement 1). Procedures based on virtual resistors [2]–[4] require an extra sensor for each virtual resistor and cannot meet the requirement 2). Procedures based on the feedback of the capacitor voltage filtered by a lead-lag network [18], [19] and high-pass filter [20] present aliasing problems when using double update mode so that the requirement 4) cannot be met. Sliding mode controllers [15], [16] require many code changes and a DSP

upgrade with faster sampling rate in order to achieve constant switching frequency so that the requirement 1) cannot be met. Adaptive control [13], [14] and neural networks [26] are sophisticated techniques that do not meet the requirement 6) simple design.

Active damping procedures based on filters at the voltage reference to the modulators are ideal candidates that meet the requirements 1), 2) and 4). The notch tuning procedure proposed in [27] uses sophisticated genetic algorithms. Reference [21] considered the notch filter, a second-order lowpass-filter, and a single lead-lag element as candidate filters. The single lead-lag element was no further considered and guidelines were provided on tuning the notch filter and the second order lag-filter. These guidelines were wide without analytical derivations so that numerous trial and error iterations were required. Reference [23] discretizes the notch filter using the bilinear transform and performs the tuning in the *z*-domain. The procedure loses much of the intuitiveness and becomes complex, also requiring trial and error iterations. Thus, the previous notch filter procedures do not meet the requirement 6) in various degrees. The procedure [22] involves a simple design, but the robustness against the line-inductance variations is limited and it may require estimating the grid inductance, so that the procedure does not meet the requirement 3). Finally, none of the previous procedures meets the requirement 5) with easy assessment of the available bandwidth.

In the search for an algorithm that meets all these requirements, this manuscript presents the following contributions:

1) Study on the equivalent grid inductance resulting from the parallel connection of three-phase grid-tie inverters.
2) New procedure for tuning the notch-filter that results in increased stability for line-inductance variations, meeting requirement 3). The design is simple without requiring trial-and-error iterations and it allows assessing how much bandwidth will be sacrificed for using active damping, meeting requirement 5). All the stated requirements are met, but the resistance of the inductors is required to be known.
3) Novel procedure for active damping based on lag-filters that displace the phase angle at the resonance frequency so that the Nyquist stability criterion is met. The procedure also allows assessing how much bandwidth will be sacrificed for using active damping, requirement 5). Thus, this proposed procedure meets all the stated requirements.

Fig. 1 shows a conceptual representation of the proposals stated in the article. This paper is organized as follows: Section II describes the control of the *LCL*-based three-phase grid-tie parallel inverters. Section III explains the proposed new tuning procedure for the notch-filter. The novel active damping procedure based on lag-filters is explained in Section IV. Simulation results are shown in Section V and experimental results with a 100 kW prototype are shown in Section VI. Section VII discusses the results and finally, Section VIII concludes the paper.
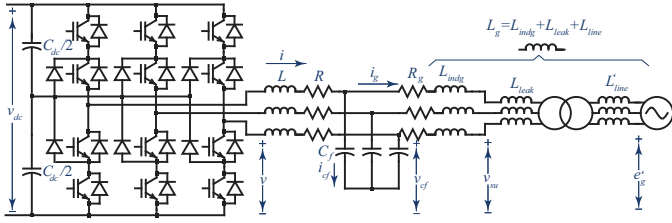
Fig. 2: Three-phase converter (three-level NPC) connected to the grid through an *LCL*-filter.

II. CONTROL OF *LCL*-BASED THREE-PHASE GRID-TIE PARALLEL INVERTERS

This section explains the stability implications of connecting multiple grid-tie converters in parallel. The section also explains the current control in the presence of additional transfer-functions in the control-loop.

Fig. 2 shows a three phase inverter connected to the grid through an *LCL*-filter where v_{dc} is DC-link voltage, C_{dc} the total DC-link capacitance, v the converter-side voltage, L the converter-side inductor inductance, R the converter-side inductor resistance, C_f the *LCL*-filter capacitor capacitance, i_{cf} the *LCL*-filter capacitor current, v_{cf} *LCL*-filter capacitor voltage, R_g the grid-side inductor resistance, i_g is the grid-side inductor current, L_{indg} the grid-side inductor inductance, L_{leak} the step-up transformer leakage inductance (referred to the low-voltage side), v_{su} the voltage at the step-up transformer terminals, L'_{line} the line-inductance (referred to the high-voltage side), and e'_g Grid voltage (referred to the high-voltage side). When referred to low-voltage side, the line-inductance and the grid voltage are L_{line} and e_g respectively. The grid-side inductance $L_g = L_{indg} + L_{leak} + L_{line}$ is defined for convenience and it combines the grid-side inductor inductance, the step-up transformer leakage inductance and the line-inductance (referred to the low-voltage side). The inverter used for the simulation and experiments of this manuscript is a three-level Neutral Point Clamped (NPC) converter, but a two-level full-bridge converter can also be used.

A. Issues of Parallel Connection of Three-phase Grid-tie Inverters

In this subsection, n parallel converters connected to the grid are considered. In the following equations the resistances of all the passive elements and the presence of step-up transformer are omitted for simplicity . The subscript ^{k} refers to each of the parallel converters. All the parallel converters share a common voltage base V_b (the voltage at the PCC) and I_b^k is the current base for the parallel converter k. If it is assumed that all the n parallel inverters have the same parameters in per unit values. The equations for each parallel converter k in per unit (base: V_b and I_b^k) are as follows:

$$\underline{v}^k = \underline{v}_{cf}^k - ls\underline{i}_k \tag{1a}$$

$$\underline{v}_{cf}^k = \underline{e}_g - \left[\underbrace{l_{line}^k\left(\sum_{j\neq k}^n \frac{I_b^j}{I_b^k}\right) + l_{line}^k}_{=l_{lineq}^k} + l_{indg}\right]s\underline{i}_g^k \tag{1b}$$

$$\underline{i}_i = c_f s\underline{v}_{cf}^k + \underline{i}_g^k \tag{1c}$$

The variables in per unit values are underlined: $\underline{v}^k$ is the converter-side voltage of the parallel converter k in per unit, $\underline{i}_{cf}^k$ the *LCL*-filter capacitor current of the parallel converter k in per unit, $\underline{v}_{cf}^k$ *LCL*-filter capacitor voltage of the parallel converter k in per unit, and $\underline{i}_g^k$ is the grid-side inductor current of the parallel converter k in per unit. The parameters in per unit are in lower case: l is the converter-side inductor inductance in per unit, c_f the *LCL*-filter capacitor capacitance in per unit, l_{indg} the grid-side inductor inductance in per unit, l_{line}^k the line-inductance expressed in per unit values using the bases V_b and I_b^k, and $\underline{e}_g$ the grid voltage in per unit. Finally s is the Laplace variable. It is also assumed that all the n parallel inverters have the same controller $c(s)$ and the same current reference per unit $\underline{i}^*$ so that:

$$\underline{v}^k = c(s)(\underline{i}^* - \underline{i}^k) \tag{2}$$

By analyzing (1), it can be seen that the parallel inverters behave as if they were connected to an equivalent line-inductance l_{lineq}^k equal to the line-inductance weighed by the rated currents I_b^k. The assumptions for the previous derivations do not consider that the switching frequency changes for different rated powers in converters so that the controllers and the parameters per unit will not be exactly the same. However, (1) gives insight into the relative influence of other parallel inverters and their rated power in the equivalent line-inductance l_{lineq}^k as seen by the individual parallel inverter. If the base currents are exactly the same for all the parallel converters $I_b^k = I_b \forall k$, then the overall line-inductance is n times the grid-inductance $l_{lineq}^k = nl_{line}$ as demonstrated by Agorreta et al. in [28].

B. Padé Approximant for Filters

Neglecting all the equivalent series resistances of the *LCL*-filter inductors and capacitor, the transfer function relating the inverter current i and voltage v is:

$$G_{LCL}(s) = \frac{i}{v} = \frac{1}{Ls}\left(\frac{s^2 + \omega_{zLC}^2}{s^2 + \omega_{res}^2}\right) \tag{3}$$

with $\omega_{zLC}^2 = (L_g C_f)^{-1}$ is the double zero of the transfer function and the $\omega_{res}^2 = L_t\omega_{zLC}^2/L$ the double pole. The resonance frequency is $f_{res} = \omega_{res}/(2\pi)$ [29].

In the double update mode [30], the sampling frequency f_s is twice the switching frequency $f_s = 2f_{sw}$ and it may result in aliasing when using active damping based on magnitude feedback. Taking into account that the effects of the integral component vanishes at the resonant frequency, the phase
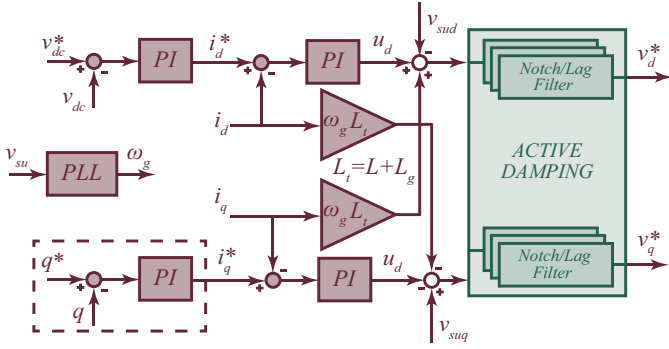
Fig. 3: Current control of the *LCL*-filter based three-phase inverter with active damping based on notch-filter/lag-filter.

angles of the resonance frequency are separated by 180 degrees and their values are [31]:

$$\varphi^+ = -\frac{\pi}{2} - 3\pi \frac{f_{res}}{f_s} \tag{4a}$$

$$\varphi^- = -\frac{3\pi}{2} - 3\pi \frac{f_{res}}{f_s} \tag{4b}$$

where f_{res} is the resonance frequency. The angles φ^+ and φ^- are shown in the Bode plot of Fig. 8.

Fig. 3 shows the overall control of the *LCL*-filter based three-phase inverter. The voltage-vector oriented controller uses a PLL to detect the grid frequency ω_g. The direct current i_d is aligned with the voltage vector and it is varied to control the active power [32]. The quadrature current i_q is perpendicular to the voltage vector and it is varied to control the reactive power. The inner controllers regulate the direct d and the quadrature q currents. The outer controller that regulates the DC-link voltage v_{dc} has the i_d^* as output. The outer controller that regulates the reactive q has the i_q^* as output. This latter controller is optional and alternatively, i_q^* can be set to zero for unity power factor.

The proposed damping procedures consists of a transfer function located after the PI controller output and before the input to the PWM modulator. This transfer function affects the low-frequency behaviour of the plant and needs to be considered in the tuning procedure of the PI controllers (this is explained in the following Subsection II-C). The bandwidth of the current-control must be lower than the resonance frequency in order to avoid interference [29], [33].

The Padé approximant $p_{N,M}(s)$ consists in a quotient of two polynomials with degree N and M in the numerator and denominator, respectively [34]. The Padé approximant $p_{N,M}(s)$ has the same Taylor series expansion as the function $f(s)$ up to degree $N + P$. The Padé approximant has been employed to approximate the low frequency behavior of transfer functions in [18], [35]. As the optimum criteria for tuning the PI controllers assumes the presence of first order systems with a single time constant, the Padé approximant $p_{0,1}(s)$ will be considered:

$$p_{0,1}(s) = \frac{1}{\tau_{Padé}s + 1} | p_{0,1}(0) = f(0) \text{ and } p'_{0,1}(0) = f'(0) \tag{5}$$

The resulting Padé approximant $p_{0,1}(s)$ has the same behaviour for the low frequency, around $s = \omega j = 0$, as the function $f(s)$.

C. Tuning Procedure for the Current Controller

The PI controller is tuned by using the low-frequency model of an *LCL*-filter, which results from neglecting the capacitor branch [18], [29]. The resulting low-frequency model is a simple *L*-filter with total inductance $L_t = L + L_g$ and the total resistance $R_t = R + R_g$. A common procedure for tuning the current-loop is the technical optimum criterion [32], [36], [37]. This method deals with a transfer function comprising two first order systems:

$$G_{lf}(s) = \frac{K}{(\tau s + 1)(Ts + 1)} \tag{6}$$

with the time constants so that $T >> \tau$ and K being a gain. In (6), the large time constant is $T = L_t / R_t$ and the smaller time constant combines the computational delay (a complete sampling cycle), the PWM delay (approximated as a half of a sampling cycle) and the time constant resulting from the Padé approximant of the transfer functions that provide active damping (notch-filter or lag-filters as explained later),

$$\tau = T_{comp} + T_{PWM} + \tau_{Padé} = T_s + 0.5T_s + \tau_{Padé} \tag{7}$$

According to the technical optimum criterion, the integration time cancels the large time constant $T_i = T$ and the proportional gain is set so to have 4% overshoot (so that the closed-loop transfer-function is a second-order system with $\xi = 0.707$ [32], a Butterworth filter with maximally flat magnitude as it corresponds to the technical optimum criterion [37]) :

$$K_p = \frac{L_t}{2\tau} \tag{8}$$

The resulting control bandwidth when using the technical optimum criterion for the PI controllers is [32]:

$$f_{bw} = \left(\frac{1}{2\pi}\right) \frac{K_p}{L_t} = \left(\frac{1}{2\pi}\right) \frac{1}{2\tau} \tag{9}$$

The control bandwidth when no active damping is included ($\tau_{Padé} = 0$ in (7)) results as follows:

$$f_{bw}^{max} = \left(\frac{1}{2\pi}\right) \frac{1}{3T_s} \tag{10}$$

The presence of the transfer functions for active damping results in a bandwidth reduction because of the additional small time constant $\tau_{Padé}$ in τ (7). The control bandwidth when the active damping procedure is included results as follows

$$f_{bw}^\tau = \left(\frac{1}{2\pi}\right) \frac{1}{3T_s + 2\tau_{Padé}} \tag{11}$$

The bandwidth reduction can be calculated by dividing (10) and (11) and it results as follows:

$$\frac{f_{bw}^{max}}{f_{bw}^{\tau}} = 1 + \frac{\tau_{Padé}}{1.5T_s} \qquad (12)$$

However, the total inductance of the *LCL*-filter is smaller than the inductance required for an *L*-filter and so lower is the voltage drop. This allows lower saturation levels in the controllers during transients due to the limited DC-link voltage ceiling.

III. NEW TUNING PROCEDURE FOR THE NOTCH-FILTER

This section explains a proposed new tuning procedure for the notch filter, which results in increased stability for line-inductance variations to meet requirement 3).

The notch-filter has a narrow notch at the resonance frequency that prevents the excitation of the *LCL*-filter resonance. In [22], it was proposed to use n notch filters in series in order to increase the width of the notch for increased robustness:

$$N_n(s) = \left(\frac{s^2 + 2D_z\omega_{nf}s + \omega_{nf}^2}{s^2 + 2D_p\omega_{nf}s + \omega_{nf}^2} \right)^{n_f} \qquad (13)$$

where ω_{nf} is the notch frequency, D_z and D_p are the damping factors for the complex conjugates poles and zeros respectively and n_f is the number of sections. The Padé approximant $p_{n\,0,1}(s)$ of the notch-filter is:

$$p_{n\,0,1}(s) = \left(\frac{1}{2\frac{D_p - D_z}{\omega_{nf}}s + 1} \right)^{n_f} \approx \frac{1}{2n_f\frac{D_p - D_z}{\omega_{res}}s + 1} \qquad (14)$$

Therefore, the resulting delay to be considered in the tuning of the PI controllers is:

$$\tau_{Padé(notch)} = \frac{2n_f}{\omega_{res}}(D_p - D_z) \qquad (15)$$

The value $n_f = 2$ was deemed reasonable in terms of proper trade-off between notch width and computational load [22]. A tolerable bandwidth reduction can be between a half or a third, which results from selecting $\tau_{Padé(noth)}$ between $1.5T_s$ and $3T_s$.

The notch frequency corresponds to the resonance frequency $\omega_n = \omega_{res}$. In [22], the damping factor D_z was selected to be zero as absolutely no component at the resonance frequency is allowed to pass through the PWM modulators. However, this criterion can be relaxed as there is always some parasitic resistance in the *LCL*-filter. For $f_s/f_{res} > 2$ by fulfilling the Nyquist frequency limit, the phase around the resonance frequency crosses $-\pi$ as $\varphi^+ > -\pi > \varphi^-$ according to (4). Hence, the resonance frequency is very close to the gain margin crossover frequency and the notch-filter should reduce the amplitude peak so the gain margin is positive:

$$|C_{PI}(j\omega_{res})||G_{pd}(j\omega_{res})||N_n(j\omega_{res})| < 0.1 \; (GM \approx \; 20 \text{ dB}) \qquad (16)$$

where $G_{pd}(s)$ is the transfer function relating the inverter voltage v and current i including all the known values (or at least a lower bound) of parasitic resistive elements (inductor resistance and capacitor filter ESR) and $C_{PI}(s)$ is the transfer function of the PI controller. A proper gain margin (GM) should be higher than 6 dB [38] and selecting 20 dB resulted in good robustness to line-inductance variations. The condition for stability is as follows:

$$|C_{PI}(j\omega_{res})||G_{pd}(j\omega_{res})| \left(\frac{D_z}{D_p} \right)^{n_f} < 0.1 \; (GM \approx \; 20 \text{ dB}) \qquad (17)$$

This relaxation in selecting D_z results in a wider notch, which will increase the stability against the line-inductance variation. The Tustin rule with pre-warping at the resonance frequency reduces the notch width of the discretized filter. The matched *z*-transform method [39] results in a notch width closer to that of the continuous case, provided the extra reduction in gain and extra phase delay still fulfills the stability conditions.

This notch filter solution requires the resistances of the inductors to be known. There is usually no control over these parameters when designing the *LCL*-filter. If there is an upgrade in the inductors, the inductance will be the same but the resistance may be different (and probably lower). In addition, the resistance of the inductors varies with the temperature. Hence, a lower bound of the resistance of the inductors is necessary to apply this active damping procedure.

IV. NOVEL ACTIVE DAMPING PROCEDURE USING LAG-FILTERS

This section explains a novel procedure for active damping based on lag-filters that fulfils the conditions stated for the target application without requiring to know the resistance of the inductors.

The proposed method uses lag-filters $G_{nlag}(s)$ to include an additional phase lag is available φ at the resonance frequency, so that the new phase angles at the resonance frequency are:

$$\varphi'^+ = \varphi^+ + \varphi \qquad (18a)$$

$$\varphi'^- = \varphi^- + \varphi \qquad (18b)$$

These angles are illustrated in Fig. 8. The values of φ required to achieve stability can be inferred from the encirclements of -1 using the Nyquist criterion. However, the stability condition is easier to infer by considering that there should be a positive real part at the resonance frequency (resistive behavior $\Re\{G_{nlag}(j\omega_{res})G_{ud}(j\omega_{res})\} > 0$). The phase angle at the resonance frequency is as follows:

$$\varphi_{res} = \frac{\varphi'^+ + \varphi'^-}{2} + \varphi = -\pi - 3\pi\frac{f_{res}}{f_s} + \varphi \qquad (19)$$

and the necessary condition for stability is $-\pi/2 < \varphi_{res} < \pi/2$. Therefore, the phase delay required for stability is:

$$-\frac{3\pi}{2} + 3\pi\frac{f_{res}}{f_s} < \varphi < -\frac{5\pi}{2} + 3\pi\frac{f_{res}}{f_s} \qquad (20)$$

Multiples of 2π have been added to (20) in order to derive the stability condition. If $\varphi_{res} = 0$ as in [40], the value of $G_{nlag}(j\omega_{res})G_{ud}(j\omega_{res})$ is real so the behavior at the resonance frequency is purely resistive.

In order to produce the required phase delay at the resonance frequency, the proposed lag-filter uses lead-lag (zero-pole) sections. The net result is a lag compensator [38] but the zero alleviates the phase-lag at lower frequencies and so the bandwidth reduction. The number of first-order lag-filters is n_l and each section will produce a phase delay $\varphi_i = \varphi/n_l$:

$$G_{nlag}(s) = \left(\frac{\frac{s}{\omega_{res}r} + 1}{\frac{rs}{\omega_{res}} + 1} \right)^{n_l} \tag{21}$$

with

$$r = \sqrt{\frac{1 - \sin(\varphi_i)}{1 + \sin(\varphi_i)}} \tag{22}$$

The resulting sections are discretized by using the Tustin method with pre-warping at the resonance frequency in order to preserve the desired characteristics in the discrete domain at the resonance frequency. Each lag section has unit amplitude at DC and a gain reduction of r^2 in the high-frequency region. The Padé approximant $p_{n\,0,1}(s)$ of the lag-filters is:

$$p_{n\,0,1}(s) = \left[\frac{1}{\frac{1}{\omega_{res}} \left(r - \frac{1}{r} \right) s + 1} \right]^{n_l} \approx \frac{1}{\frac{n_l}{\omega_{res}} \left(r - \frac{1}{r} \right) s + 1} \tag{23}$$

Therefore, the resulting delay to be considered in the tuning of the PI controllers is:

$$\tau_{Padé(nlag)} = \frac{n_l}{\omega_{res}} \left(r - \frac{1}{r} \right) \tag{24}$$

The number of lag-filters n_l must result in $|\varphi_i| < \pi/2$. For a fixed value of φ, a higher number of sections n_l results in a smaller delay in (24) because the term depending on r (22) decays faster than n_l. Therefore, increasing the number of sections n_l will increase bandwidth by reducing (24). However, these improvements are at the expense of more computations. Making $n_l = 4$ results in approximately the same number of computations as in the previous second order notch filter and it provides a reasonable trade-off between bandwidth reduction and processing time.

The phase margin PM in degrees is related to the phase delay φ as follows (see Figs. 5 and 8):

$$\varphi = (PM - 180)\frac{2\pi}{360} + \left(-\frac{3\pi}{2} + 3\pi\frac{f_{res}}{f_s} \right) \tag{25}$$

This formula can be used to select the PM for the nominal resonance frequency. However, the increase in the line-inductance L_l and the increase of the number of parallel inverters increases the grid inductance L_g and reduces the resonance frequency f_{res}. The proper tuning procedure should consider a minimum adequate PM (between 30 and 60

TABLE I: Parameters of the set-up used for simulations and experiments.

Grid-tie inverter		
Rated power	S_n	100 kVA
Rated ac voltage	V_n	400 V
Rated frequency	f_n	50 Hz
dc link voltage	v_{DC}	700 V
Sampling frequency	f_s	5100 Hz
PWM frequency	f_{sw}	2550 Hz
LCL- filter		
Inverter coil inductance	L	0.5 mH (5.67 %)
Inverter coil resistance	R	4.7 mΩ (0.17 %)
Filter capacitor	C_f	33 μF (2.9 %)
Grid coil inductance	L_g	0.25 mH (2.8 %)
Grid coil resistance	R_g	2.36 mΩ (0.09 %)
Resonance frequency	f_{res}	2135 Hz

degrees [38]) for the maximum realistic increase in the line-inductance which results in the minimum resonant frequency f_{res}^{min}. The prover value for φ is calculated by substituting the selected PM for the minimum resonance frequency in (25), yet the system must have a reasonable PM for the nominal resonance frequency. If the resulting PM for the nominal resonance frequency is too small, the worst condition f_{res}^{min} cannot be fulfilled and the PM should be increased.

V. SIMULATION RESULTS

Table I shows all the data of the set-up used for simulations and experiments. The design procedure for the *LCL*-filter design is explained in [29]. The ratio $L_g/L = 1.6$ was selected in [29], but in this manuscript the value of the grid-side inductance L_g is varied from an initial value of 0.25 mH ($L_g/L = 0.5$) to a final value of 2.5 mH ($L_g/L = 5$) in order to study the variations in the line-inductance. The simulation software is Matlab/Simulink/SimPowerSystems and the semiconductor switches are ideal. The values of the *LCL*-filter parameters presented in Table I result from applying the design procedure explained in [29]. The experiments will be performed in a scaled 100 kVA three-level NPC converter whereas the target industrial application uses an 800 kVA two-level converter. The voltage is measured at the filter capacitor terminals and is used for grid synchronization. For the initial value of L_g, the ratio between $f_s/f_{res} = 2.4$ is very close to the Nyquist limit. In addition, sudden increments in the grid inductance will be considered that may be due to additional line-inductance or due to the connection of additional parallel inverters [28]. In both situations, achieving stability is a challenging task for the active damping procedure.

A. New Tuning Procedure for the Notch-filter

Previous references [18], [22] considered a bandwidth reduction of no more than 2 when using active damping. A bandwidth reduction of 2.64 times was selected for the notch-filter procedure; simulations and experiments will show that the resulting bandwidth was sufficient for tracking the sinusoidal reference in the current-loop. Solving (12) results in $\tau_{Padé(notch)} = 2.46T_s$. The required parameters of the notch-filter $D_p = 1.7$ and $D_z = 8.86e - 2$ are calculated by using (15) and (17) for $n_f = 2$ as explained in Section III.
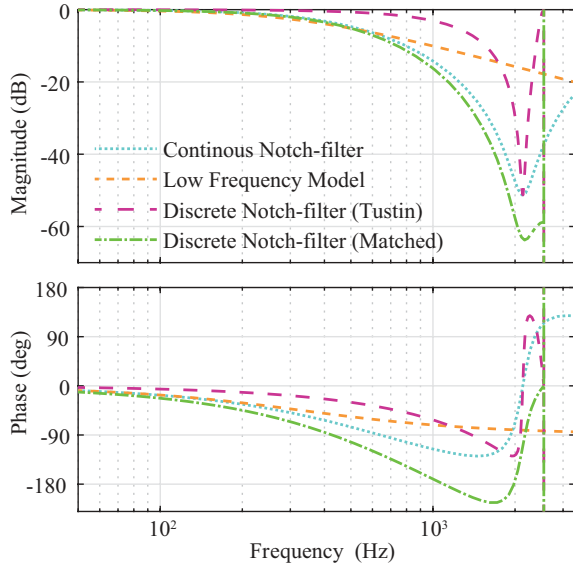
Fig. 4: Frequency response of the continuous notch-filter, the discrete notch-filter using the Tustin rule with pre-warping at the resonance frequency and the discrete notch-filter using the matched z-transform rule.

Fig. 5: Bode plot for the open-loop transfer function with no notch-filter (no active damping procedure), the notch-filter using the Tustin rule and the notch-filter using the matched z-transform rule. The figure also shows the open-loop transfer function for the low-frequency model.

Fig. 5 shows the Bode plot for the open-loop transfer function with no notch-filter (no active damping procedure), the notch-filter using the Tustin rule and the notch-filter using the matched z-transform rule. It can be seen that the system is unstable when no notch-filter (no active damping procedure) is included. The overall system is stable when the notch-filter using the Tustin rule is included. The gain margin crossover frequency is still approximately at the resonance frequency (as explained in Section III) and the gain margin is positive rendering the overall system stable. The overall system is also stable when the notch-filter uses the matched z-transform and it has a wider notch. This will result in increased robustness against resonance frequency variations due to changing line-impedance. Fig. 5 also shows the Bode plot for the low-frequency model that neglects the *LCL*-filter branch capacitor and uses the Padé approximant of the notch-filter, which is very close to the exact model in the low-frequency region.

The minimum GM and PM are also shown in Fig. 5. It can be seen that the control-loop is unstable when the active damping procedure is not present with negative GM at the resonance frequency. After including the notch filter, the GM at the resonance frequency is positive and 23.7 dB; close to the selected 20 dB in (17). The minimum GM and PM are respectively 11.4 dB and 52.4 degrees for the case using the Tustin rule. For the case of the z-transform matched rule, the minimum GM and PM are respectively 5.8 dB and 28.7 degrees. The minimum stability margins are lower for the z-transform matched rule, but still around the recommended 6 dB and 30 degrees [38].

B. Novel Active Damping Procedure based on Lag-filters

For the multiple lag-filters, a phase margin $PM = 30$ degrees is considered adequate when the grid inductance L_g
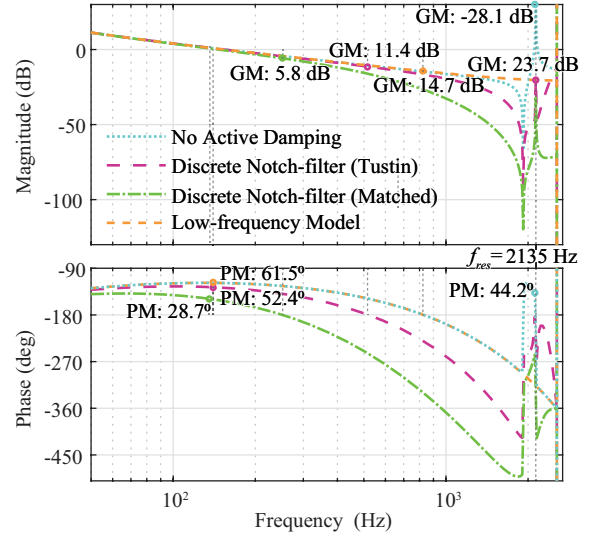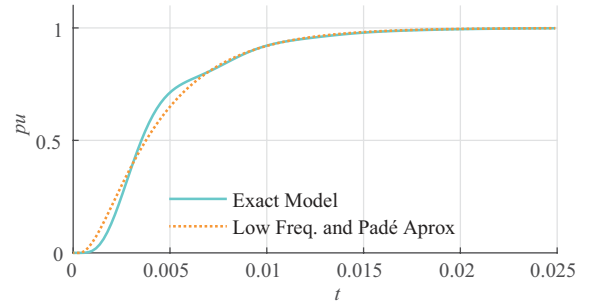

Fig. 6: Step response of the exact model and approximate model using the *LCL*-filter low-frequency model and the Padé approximant of the lag-filters.

is nine times the initial value (this situation corresponds to the minimum resonance frequency $f_{res}^{min} = 1362.9$ Hz). This results in $\varphi = -155.7$ degrees by substituting in (25) and $\varphi_i = -38.9$ degrees ($r = 2.09$ according to (22)) by selecting $n_l = 4$ in order to have the same number of computations as in the notch-filter case.

The resulting delay $\tau_{Padé(nlag)} = 2.46T_s$ is calculated with (24) and entails an acceptable bandwidth reduction of 2.6 times (same as in the notch-filter case). For this case as well it is required to use the low-frequency model that neglects the *LCL*-filter capacitor branch and uses the Padé approximant of the lag-filters in order to tune the PI controllers according to (8). Fig. 6 compares the step responses of the exact model and the low-frequency model that neglects the *LCL*-filter capacitor branch and uses the Padé approximant of the lag-filters (without loss of generality, the PI controller gains were tuned to result in no overshoot). The lag filters also produce some initial warping, but the step-responses are very similar with the same settling time and the approximation method is validated.
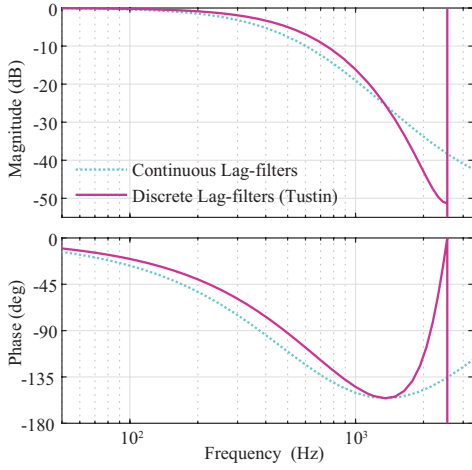
Fig. 7: Frequency response of the continuous lag-filters and the discrete lag-filters using the Tustin rule with pre-warping at the resonance frequency.
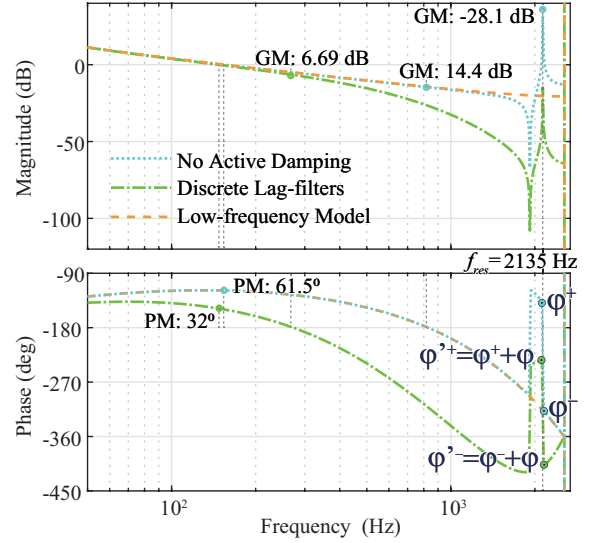

Fig. 8: Bode plot for the open-loop transfer function with no lag-filters (no active damping procedure) and the lag-filters for active damping. The figure also shows the open-loop transfer function for the low-frequency model.

Fig. 7 shows the frequency response of the continuous lag-filters and the discrete lag-filters using the Tustin rule with pre-warping at the resonance frequency. There is an exact match between the discrete and continuous models around the resonance frequency as expected. Unlike the notch-filter case, the discrete lag-filters do not result in an estimable width reduction.

Fig. 8 shows the Bode plot for the open-loop transfer function with no lag-filters (no active damping procedure) and the lag-filters using the Tustin rule. It can be seen that the system is unstable when no lag-filters (no active damping procedure) are included. When the lag-filters are inserted, the overall system is stable and the selection of $PM = 30$ degrees for the maximum grid inductance was adequate. Fig. 8 also shows the Bode plot for the low-frequency model that neglects the LCL-filter branch capacitor and uses the Padé approximant of the notch-filter, which is very close to the exact model in the low-frequency region. The minimum GM and PM are also shown in Fig. 8. The control-loop is unstable when the active damping procedure is not present with negative GM at the resonance frequency. The minimum GM and PM are respectively 6.69 dB and 32 degrees, slightly higher than the recommended 6 dB and 30 degrees [38].

Fig. 9 shows the root locus in the z-plane when varying L_g from 75% to 1000% of the initial value (from 0.2 mH to 2.5 mH) for the case of the lag-filters. The overall system is stable for the whole range of L_g variation around the initial value. This is because the design procedure considered the stability for the worst case with $PM = 30$ degrees when the grid inductance L_g is nine times the initial value.

Fig. 10 shows the simulation results for the notch-filter case using the z-plane. The only parasitic resistances considered are R and R_g, the extra line-inductance is purely inductive. The current-loop cannot be stable by the passive damping provided by these limited resistance values and active damping is required. The current-loop is stable for all the situations, but the system resonates for the initial inductance value of
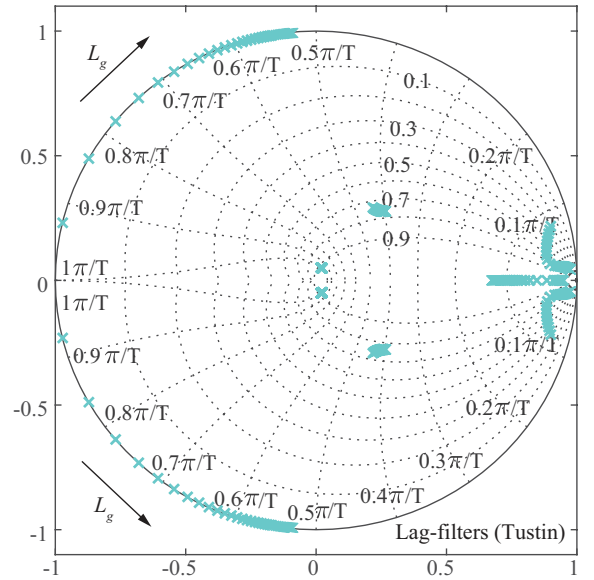
Fig. 9: root locus in the z-plane when varying L_g from 80% to 1000% (from 0.2 mH to 2.5 mH) for the lag-filter using the Tustin rule with pre-warping.

L_g. This is because the sampling frequency is very close (2.4 times) to the resonance frequency and the achieved damping is not sufficient. Active damping algorithms usually require that the sampling frequency be more than 3 times the resonance frequency [41]. After three cycles, an extra inductance of 9 times the initial inductance L_g (2.25 mH) is connected and the current-loop remains stable, which demonstrates the robustness of the proposed new active damping procedure based on lag-filters. The current harmonic distortion improves considerably from THD=52% to THD=0.47% because of this extra inductance. Finally, after eight cycles the active damping mechanism is deactivated and the current-loop becomes unstable as expected.
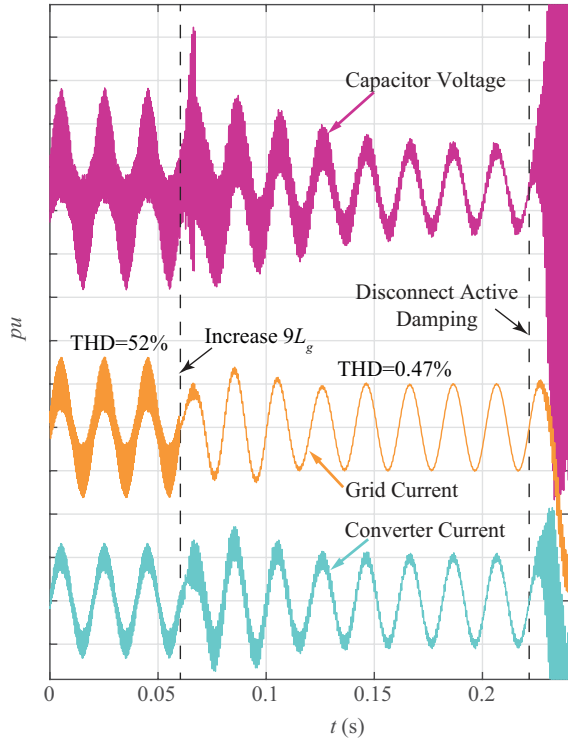
Fig. 10: Simulation results for the lag-filters using the Tustin rule with pre-warping.

Finally, it should be mentioned that unsuccessful attempts were made to use well-established procedures for active damping [41]. This remarks that the proposed procedures were successful in the face of difficult conditions to achieve stability with the *LCL*-filter based three-phase NPC inverter using the parameters shown in Table I.

VI. EXPERIMENTAL RESULTS

Fig. 11 shows a picture of the 100 kVA set-up used for the experiments. The three-level NPC grid-tie inverter is directly connected to a Regatron programmable three-phase power supply. The initial value of the grid inductance L_g is 0.25 mH ($L_g = 0.5L$) and during the tests the grid inductance is increased up to 0.75 mH in a first step and up to 1.25 mH ($L_g = 2.5L$) in a second step. The grid inductance increments are sudden by opening the bypass breakers that short-circuit extra inductors.

Figs. 12-14 show the oscilloscope captures when the active damping procedure based on lag-filters is connected. Fig. 12 shows the grid voltage and the current waveforms after a 25 Amp step change in the current reference. The response is critically damped and consistent with the simulation shown in Fig. 6. The system behavior is stable but the current exhibits a large ripple because the switching frequency is very close (1.2 times) to the resonance frequency. The experiments are fully consistent with the simulations shown in Fig. 10. Fig. 13 shows the grid voltage and current waveforms for the sudden addition of extra line-inductance with a value twice the initial value of L_g (0.5 mH). At the beginning of this experiment,
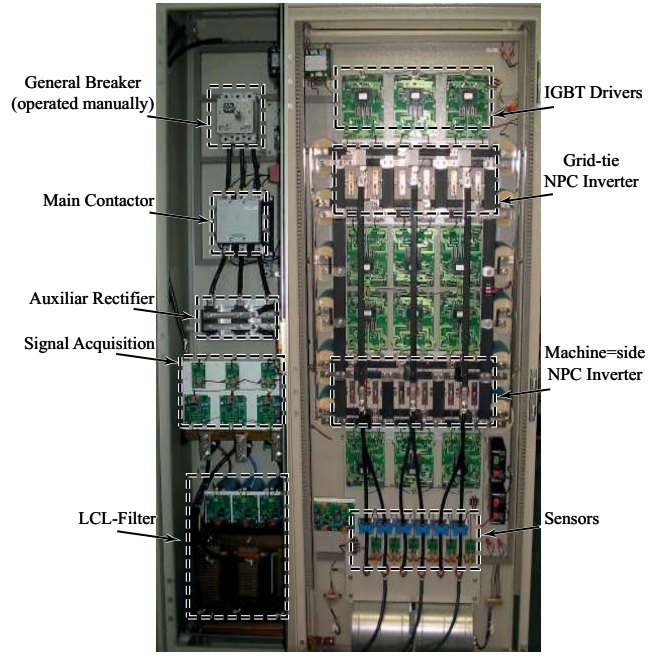

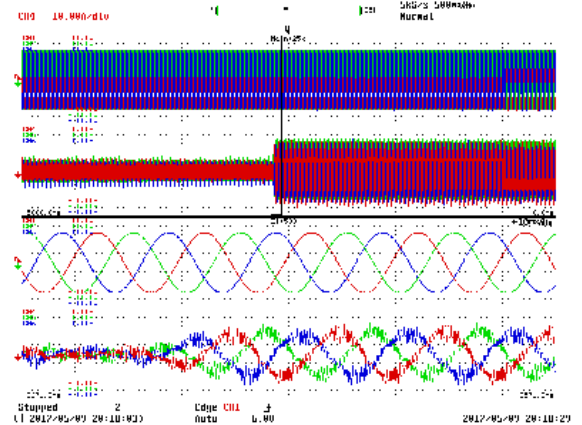Fig. 11: 100 kVA Experimental set-up.

Fig. 12: Experimental results for the lag-filters: grid voltage and current waveforms for a 25 Amp current reference step.

the grid inductance L_g has its the initial value (0.25 mH). After adding the extra line-inductance, the grid inductance L_g is three times its initial value (0.75 mH). The system remains stable and the current harmonics are reduced due to the filtering capability of the additional inductance. Finally, Fig. 14 shows the grid voltage and current waveforms for another sudden addition of extra line-inductance with a value twice the initial value of L_g (0.5 mH). At the beginning of this experiment, the grid inductance is three times its initial value of L_g (0.75 mH). After adding another extra line-inductance, the grid inductance L_g is five times the initial value (1.25 mH). The system remains stable with a grid inductance L_g of 5 times its initial value (1.25 mH), which demonstrates the robustness against line-inductance variations of the proposed novel active damping procedure based on lag-filters.

For both cases, experiments are fully consistent with theoretical derivations and simulations. The experiments present
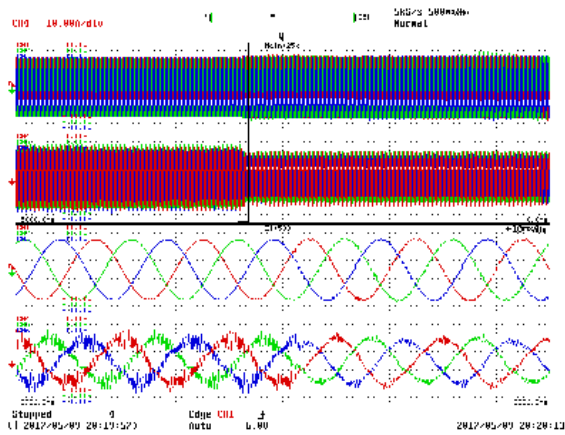
Fig. 13: Experimental results for the lag-filters: grid voltage and current waveforms for the sudden addition of extra line-inductance with a value twice the initial value of L_g (0.5 mH). At the beginning of this experiment, the grid inductance has its the initial value L_g (0.25 mH). After adding the extra line-inductance, the grid inductance L_g is three times its initial value (0.75 mH).
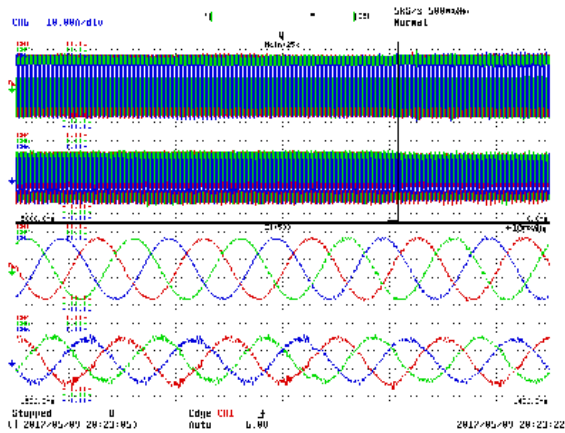

Fig. 14: Experimental results for the lag-filters: grid voltage and current waveforms for the sudden addition of another extra line-inductance with a value twice the initial value of L_g (0.5 mH). At the beginning of this experiment, the grid inductance L_g is three times its initial value (0.75 mH). After adding another extra line-inductance, the grid inductance L_g is five times its initial value (1.25 mH).

additional damping because of the non-modeled dissipative elements (cores losses, capacitor ESR, inverter losses,...).

VII. DISCUSSION

The numerous requirements stated for this industrial application are very constraining and the procedure presents limitations and trade-offs in the results. The maximum bandwidth f_{bw}^{max} is determined by (10) and the switching frequency is the limiting factor. The switching frequency is limited in medium voltage converters so to reduce the switching losses in the semiconductors. The proposed procedures allow selecting the amount of bandwidth to be sacrificed for using active damping; the final bandwidth f_{bw}^{τ} is determined by (12). In this case, the trade-off is between bandwidth reduction and robustness to line-inductance variations. The bandwidth of the current-controllers must be sufficient to track the sinusoidal reference and, in certain cases, to cancel a specific harmonic component

as for example if there is substantial harmonic content in the grid voltage.

The main disadvantage of the procedure is that the damping many not be sufficient for very low values of L_g/L. Even though the current-loop is stable for all range of L_g variation, the system resonates in the simulation results for the initial L_g with the sampling frequency is very close (2.4 times) to the resonance frequency. However, the system will never work with the initial inductance value $L_g = 0.25$ mH ($L_g/L = 0.5$) as that the wind-turbine manufacturer assumes some known values for the line-impedance in order to minimize the grid-side inductor size. The system achieved a THD< 5% for $L_g = 0.9L$ ($L_g = 0.45$ mH, 1.8 times the initial value of L_g). For the ratio $L_g/L = 1.6$ as selected in [29], the THD achieved is 1.57%.

The results in the simulations and experiments for the notch-filter (using the z-transform matched rule) are very similar to those of the lag-filter. The root locus analysis in the z-plane shows that the system is stable for the whole range for L_g varying from 80% to 1000%. In the simulation results, the systems initially resonated with THD=52% with the sampling frequency is very close (2.4 times) to the resonance frequency and finally it achieves a THD=0.47% after applying 9 times the initial inductance L_g (2.25 mH). The system achieves a THD<5% for $L_g/L = 0.8$ ($L_g = 0.4$ mH, 1.6 times the initial value of L_g). For the ratio $L_g/L = 1.6$ as selected in [29], the THD achieved is 1.53%. The main disadvantage of this the notch filter procedure is the necessity of knowing the resistance of the inductors.

VIII. CONCLUSION

This paper present a list of requirements for active damping in *LCL*-filter based medium-voltage grid-tie parallel inverters. The proposed solutions use filters in the voltage reference to the modulator. The presented approach allows selecting the bandwidth to be sacrificed for using active damping by calculating the Padé aproximant. The proposed tuning procedure for the notch-filter increases the robustness against the line-impedance variations using a simple design procedure that that requires to know the resistance of the inductors. The method of the lag-filters selects the phase margin for the worst case increase in the grid inductance to guarantee stability. Therefore, this proposed procedure constitutes an appropriate solution for this industrial application related to wind energy.

REFERENCES

[1] R. Pena-Alzola, M. Liserre, F. Blaabjerg, R. Sebastian, J. Dannehl, and F. Fuchs, "Analysis of the passive damping losses in lcl-filter-based grid converters," *IEEE Trans. Power Electron.*, vol. 28, no. 6, pp. 2642–2646, June 2013.

[2] P. A. Dahono, "A control method to damp oscillation in the input lc filter," in *2002 IEEE 33rd Annu/ IEEE Power Electron. Specialists Conf. Proc. (Cat. No.02CH37289)*, vol. 4, 2002, pp. 1630–1635.

[3] X. Wang, F. Blaabjerg, and P. C. Loh, "Virtual rc damping of lcl-filtered voltage source converters with extended selective harmonic compensation," *IEEE Trans. Power Electron.*, vol. 30, no. 9, pp. 4726–4737, Sept 2015.

[4] ——, "Grid-current-feedback active damping for lcl resonance in grid-connected voltage-source converters," *IEEE Trans. Power Electron.*, vol. 31, no. 1, pp. 213–223, Jan 2016.

[5] V. Miskovic, V. Blasko, T. M. Jahns, A. H. C. Smith, and C. Romenesko, "Observer-based active damping of lcl resonance in grid-connected voltage source converters," *IEEE Trans. Ind. Applicat.*, vol. 50, no. 6, pp. 3977–3985, Nov 2014.

[6] Y. Lyu, H. Lin, and Y. Cui, "Stability analysis of digitally controlled lcl-type grid-connected inverter considering the delay effect," *IET Power Electron.*, vol. 8, no. 9, pp. 1651–1660, 2015.

[7] J. Wang, J. D. Yan, L. Jiang, and J. Zou, "Delay-dependent stability of single-loop controlled grid-connected inverters with lcl filters," *IEEE Trans. Power Electron.*, vol. 31, no. 1, pp. 743–757, Jan 2016.

[8] C. Chen, J. Xiong, Z. Wan, J. Lei, and K. Zhang, "A time delay compensation method based on area equivalence for active damping of an lcl -type converter," *IEEE Trans. Power Electron.*, vol. 32, no. 1, pp. 762–772, Jan 2017.

[9] R. Guzman, L. G. de Vicua, J. Morales, A. Momeneh, J. Miret, and J. Torres-Martnez, "Active damping based on ackermann's formula for a three-phase voltage source inverter with lcl filter," in *ICON 2015 - 41st Annu. Conf. of the IEEE Ind. Electron. Soc.*, Nov 2015, pp. 001 217–001 222.

[10] D. Perez-Estevez, J. Doval-Gandoy, A. G. Yepes, and O. Lopez, "Positive- and negative-sequence current controller with direct discrete-time pole placement for grid-tied converters with lcl filter," *IEEE Trans. Power Electron.*, vol. PP, no. 99, pp. 1–1, 2016.

[11] F. Huerta, D. Pizarro, S. Cobreces, F. J. Rodriguez, C. Giron, and A. Rodriguez, "Lqg servo controller for the current control of lcl grid-connected voltage-source converters," *IEEE Trans. Ind. Electron.*, vol. 59, no. 11, pp. 4272–4284, Nov 2012.

[12] J. Roldan-Perez, A. Garcia-Cerrada, J. L. Zamora-Macho, and M. Ochoa-Gimenez, "Helping all generations of photo-voltaic inverters ride-through voltage sags," *IET Power Electron.*, vol. 7, no. 10, pp. 2555–2563, 2014.

[13] M. Andresen, M. Liserre, F. W. Fuchs, and N. Hoffmann, "Design of a grid adaptive controller for pwm converters with lcl filters," in *IECON 2015 - 41st Annu. Conf. of the IEEE Ind. Electron. Soc.*, Nov 2015, pp. 003 664–003 671.

[14] J. Kukkola and M. Hinkkanen, "State observer for grid-voltage sensor-less control of a converter equipped with an lcl filter: Direct discrete-time design," *IEEE Trans. Ind. Applicat.*, vol. 52, no. 4, pp. 3133–3145, July 2016.

[15] H. Komurcugil, S. Ozdemir, I. Sefa, N. Altin, and O. Kukrer, "Sliding-mode control for single-phase grid-connected mboxLCL -filtered vsi with double-band hysteresis scheme," *IEEE Trans. Ind. Electron.*, vol. 63, no. 2, pp. 864–873, Feb 2016.

[16] R. Guzman, L. G. de Vicuna, J. Morales, M. Castilla, and J. Miret, "Model-based active damping control for three-phase voltage source inverters with lcl filter," *IEEE Trans. Power Electron.*, vol. PP, no. 99, pp. 1–1, 2016.

[17] J. Dannehl, F. W. Fuchs, S. Hansen, and P. B. Thogersen, "Investigation of active damping approaches for pi-based current control of grid-connected pulse width modulation converters with lcl filters," *IEEE Trans. Ind. Applicat.*, vol. 46, no. 4, pp. 1509–1517, July 2010.

[18] R. Pena-Alzola, M. Liserre, F. Blaabjerg, R. Sebastin, J. Dannehl, and F. W. Fuchs, "Systematic design of the lead-lag network method for active damping in lcl-filter based three phase converters," *IEEE Trans. Ind. Informat.*, vol. 10, no. 1, pp. 43–52, Feb 2014.

[19] V. Blasko and V. Kaura, "A novel control to actively damp resonance in input lc filter of a three-phase voltage source converter," *IEEE Trans. on Ind. Applicat.*, vol. 33, no. 2, pp. 542–550, Mar 1997.

[20] X. Bao, F. Zhuo, Y. Tian, and P. Tan, "Simplified feedback linearization control of three-phase photovoltaic inverter with an lcl filter," *IEEE Trans. Power Electron.*, vol. 28, no. 6, pp. 2739–2752, June 2013.

[21] J. Dannehl, M. Liserre, and F. W. Fuchs, "Filter-based active damping of voltage source converters with lcl filter," *IEEE Trans. Ind. Electron.*, vol. 58, no. 8, pp. 3623–3633, Aug 2011.

[22] R. Pena-Alzola, M. Liserre, F. Blaabjerg, M. Ordonez, and T. Kerekes, "A self-commissioning notch filter for active damping in a three-phase lcl -filter-based grid-tie converter," *IEEE Trans. Power Electron.*, vol. 29, no. 12, pp. 6754–6761, Dec 2014.

[23] W. Yao, Y. Yang, X. Zhang, F. Blaabjerg, and P. C. Loh, "Design and analysis of robust active damping for lcl filters using digital notch filters," *IEEE Trans. Power Electron.*, vol. 32, no. 3, pp. 2360–2375, March 2017.

[24] J. Y. Hung, "Feedback control with posicast," *IEEE Trans. Ind. Electron.*, vol. 50, no. 1, pp. 94–99, Feb 2003.

[25] A. Vidal, A. G. Yepes, F. D. Freijedo, . Lpez, J. Malvar, F. Baneira, and J. Doval-Gandoy, "A method for identification of the equivalent inductance and resistance in the plant model of current-controlled grid-tied converters," *IEEE Trans. Power Electron.*, vol. 30, no. 12, pp. 7245–7261, Dec 2015.

[26] X. Fu and S. Li, "Control of single-phase grid-connected converters with lcl filters using recurrent neural network and conventional control methods," *IEEE Trans. Power Electron.*, vol. 31, no. 7, pp. 5354–5364, July 2016.

[27] M. Liserre, A. Dell'Aquila, and F. Blaabjerg, "Genetic algorithm-based design of the active damping for an lcl-filter three-phase active rectifier," *IEEE Trans. Power Electron.*, vol. 19, no. 1, pp. 76–86, Jan 2004.

[28] J. L. Agorreta, M. Borrega, J. Lpez, and L. Marroyo, "Modeling and control of n -paralleled grid-connected inverters with lcl filter coupled due to grid impedance in pv plants," *IEEE Trans. Power Electron.*, vol. 26, no. 3, pp. 770–785, March 2011.

[29] M. Liserre, F. Blaabjerg, and S. Hansen, "Design and control of an lcl-filter-based three-phase active rectifier," *IEEE Trans. Ind. Applicat.*, vol. 41, no. 5, pp. 1281–1291, Sept 2005.

[30] V. Blasko, V. Kaura, and W. Niewiadomski, "Sampling of discontinuous voltage and current signals in electrical drives: a system approach," *IEEE Transactions on Industry Applications*, vol. 34, no. 5, pp. 1123–1130, Sep 1998.

[31] Y. Tang, W. Yao, P. C. Loh, and F. Blaabjerg, "Design of lcl filters with lcl resonance frequencies beyond the nyquist frequency for grid-connected converters," *IEEE J. of Emerging and Select. Topics in Power Electron.*, vol. 4, no. 1, pp. 3–14, March 2016.

[32] V. Blasko and V. Kaura, "A new mathematical model and control of a three-phase ac-dc voltage source converter," *IEEE Trans. Power Electron.*, vol. 12, no. 1, pp. 116–123, Jan 1997.

[33] M. L. *, F. Blaabjerg, and A. DellAquila, "Step-by-step design procedure for a grid-connected three-phase pwm voltage source converter," *International Journal of Electronics*, vol. 91, no. 8, pp. 445–460, 2004.

[34] W. Yang, W. Cao, T. Chung, and J. Morris, *Applied Numerical Methods Using MATLAB*. Wiley, 2005.

[35] R. Pena-Alzola, D. Campos-Gaona, P. F. Ksiazek, and M. Ordonez, "Dc-link control filtering options for torque ripple reduction in low-power wind turbines," *IEEE Trans. Power Electron.*, vol. 32, no. 6, pp. 4812–4826, June 2017.

[36] W. Leonhard, *Control of Electrical Drives*, ser. Engineering library. Springer Berlin Heidelberg, 2001.

[37] J. W. Umland and M. Safiuddin, "Magnitude and symmetric optimum criterion for the design of linear control systems: what is it and how does it compare with the others?" *IEEE Trans. Ind. Applicat.*, vol. 26, no. 3, pp. 489–497, May 1990.

[38] K. Ogata, *Modern Control Engineering*, ser. Instrumentation and controls series. Prentice Hall, 2010.

[39] E.-K. Press, G. Franklin, J. Powell, and M. Workman, *Digital Control of Dynamic Systems*. Ellis-Kagle Press, 1998.

[40] J. Roldan-Perez, E. Bueno, and A. Rodriguez-Cabero, "A simplified active damping method for grid-connected converters with lcl filters," in *IEEE Energy Conversion Congr. and Expo. ECCE' 2017*, 2017.

[41] R. Pena-Alzola, M. Liserre, F. Blaabjerg, M. Ordonez, and Y. Yang, "Lcl-filter design for robust active damping in grid-connected converters," *IEEE Trans. Ind. Informat.*, vol. 10, no. 4, pp. 2192–2203, Nov 2014.

Rafael Peña Alzola Rafael Peña-Alzola received the combined licentiate and M.Sc. degree in industrial engineering from the University of the Basque Country, Bilbao, Spain, in 2001, and the Ph.D. degree from the National University for Distance Learning (UNED), Madrid, Spain, in 2011. He has worked as an electrical engineer for several companies in Spain. From September 2012 to July 2013, he was Guest Postdoc at the Department of Energy Technology at Aalborg University in Aalborg, Denmark. From August 2014 to December 2016, he was Postdoc Research Fellow at the Department of Electrical and Computer Engineering at The University of British Columbia in Vancouver, Canada. From January 2017 to May 2017, he was with the University of Alcalá in Madrid, Spain for a short-term industrial collaboration.

Since June 2017, he is Research Fellow at the Rolls Royce University Technology Centre at the University of Strathclyde in Glasgow, UK. His research interests are energy storage, LCL-filters, solid-state transformers, power electronics for hybrid electric aircraft and innovative control techniques for power converters.

David Campos-Gaona David Campos-Gaona (M'12) received the B.E. degree in electronic engineering, and the M.Sc. and Ph.D. degrees in electrical engineering, all from Instituto Tecnolgico de Morelia, Morelia, Mexico, in 2004, 2007, and 2012, respectively. From 2014 to 2016, he was a Postdoctoral Research Fellow with the Department of Electrical and Computer Engineering, University of British Columbia, Vancouver, Canada. Since August 2016, he is a Research Associate with the University of Strathclyde, Glasgow, U. K. His research interest include wind farm power integration, HVDC transmission systems, and real-time digital control of power-electronic-based devices.

Javier Roldán-Pérez Javier Roldán-Pérez received a B.S. degree in industrial engineering, a M.S. degree in electronics and control systems, a M.S. degree in system modeling, and a Ph.D. degree in power electronics, all from Comillas Pontifical University, Madrid, in 2009, 2010, 2011, and 2015, respectively. From 2010 to 2015, he was with the Institute for Research in Technology (IIT), Comillas University. In 2014, he was a visiting Ph.D. student at the Department of Energy Technology, Aalborg University, Denmark. From 2015 to 2016 he was with the Electric and Control Systems Department at Norvento Energa Distribuida. In September 2016 he joined the Electrical Systems Unit at IMDEA Energy Institute, where his research topics are the integration of renewable energies, microgrids, and power electronics applications.

Marco Liserre Marco Liserre (S'00-M'02-SM'07-F'13) received the MSc and PhD degree in Electrical Engineering from the Bari Polytechnic, respectively in 1998 and 2002. He has been Associate Professor at Bari Polytechnic and Professor at Aalborg University (Denmark). He is currently Full Professor and he holds the Chair of Power Electronics at Christian-Albrechts-University of Kiel (Germany). He has published over 300 technical papers (more than 100 of them in international peer-reviewed journals) and a book. These works have received more than 20,000 citations. Marco Liserre is listed in ISI Thomson report The worlds most influential scientific minds. He is member of IAS, PELS, PES and IES. He has been serving all these societies in different capacities and he has received several IEEE awards.

Emilio Bueno Emilio J. Bueno (S'05-M'06) was born in Madrid, Spain, in 1972. He received the M.S. and Ph.D. degrees in electronics engineering from the University of Alcalá, Alcalá de Henares, Spain, in 1999 and 2005, respectively. Since 2009, he has been an Associate Professor with the Department of Electronics, University of Alcalá, and a member of the Electronics Engineering Applied to Renewable Energies Research Group.

From 2010 to 2013, he was a Vice-Dean of the Polytechnic School, University of Alcalá, in charge of electrical engineering studies. His research interests include linear control of grid converters and drives, power quality, distributed generation systems, and medium-voltage converter topologies.

Graeme Burt Graeme M. Burt (M'95) received the B.Eng. degree in electrical and electronic engineering, and the Ph.D. degree in fault diagnostics in power system networks from the University of Strathclyde, Glasgow, U.K., in 1988 and 1992, respectively. He is currently a Professor of electrical power systems at the University of Strathclyde where he co-directs the Institute for Energy and Environment, directs the Rolls-Royce University Technology Centre in Electrical Power Systems, and is lead academic for the Power Networks Demonstration Centre (PNDC). In addition, he serves as spokesperson for the board of DERlab e.V., the association of distributed energy laboratories. His research interests include the areas of power system protection and control, distributed energy, and experimental validation.

Francisco Huerta Francisco Huerta (S'08-M'11) received the M.Sc. degree and the Ph.D. degree in electronics engineering from the University of Alcalá, Alcalá de Henares, Spain, in 2006 and 2011, respectively.

He worked as a Research Assistant from 2007 and 2012 with the University of Alcalá. From 2013 until 2016, he was a Postdoctoral Researcher with Institute IMDEA Energy. From 2016 to 2017, he worked as a Researcher with the University of Alcalá. Currently he is an Assistant Professor with the Carlos III University of Madrid. His research interests include control of power electronics converters, power quality and distributed power generation systems.